The Seismic 8° Discontinuity and Partial Melting in Continental Mantle

H. Thybo* and E. Perchuć

Strong, scattered reflections beyond 8 degrees (8°) offset are characteristic features of all high-resolution seismic sections from the continents. The reflections identify a low-velocity zone below approximately 100 kilometers depth beneath generally stratified mantle. This zone may be caused by partial melting, globally initiated at equal depth in the continental mantle. Solid state is again attained at the Lehmann discontinuity in cold, stable areas, whereas the zone extends to near the 400-kilometer discontinuity in hot, tectonically active areas. Thus, the depth to the Lehmann discontinuity may be an indicator of the thermal state of the continental mantle.

Three fundamental seismic discontinuities in the outer 1000 km of the Earth are well established from seismological data: the Mohorovicic discontinuity (Moho), the 400-km discontinuity, and the 650-km discontinuity (*1*). Another discontinuity, the Lehmann discontinuity, was originally interpreted at a depth of ~220 km below Europe from earthquake data and below the North American craton from GNOME nuclear explosion data (*2*). Other seismic studies of cratonic areas have identified similar discontinuities at ~220 km (150 to 280 km) depth with positive velocity contrasts (*3*), whereas studies of noncratonic areas do not reveal such a discontinuity (*4*). Recent interpretations of the Lehmann discontinuity have focused on an abrupt change in anisotropy (*5*) or disappearance of a zone of partial melting (*6*). Zones of high- and low-velocity layers in the uppermost mantle below the Moho are well established (*7*, *8*). Recently, a characteristic change in seismic structure at a depth of ~100 km below the Baltic Shield was interpreted (*9*). Here, we extend this interpretation and present seismic and seismological evidence for "the 8° Discontinuity" at a depth of ~100 km. The discontinuity is identified in all available seismic, long-range profiles, which indicates that it is a global characteristic of the continental mantle.

The 8° discontinuity is identified from a change in seismic character at ~8° (700 to 900 km) offset. It cannot be identified from single seismograms or low-density record sections because of the negative contrast in seismic velocity across the discontinuity. Detection was possible because of access to high-density, long-range seismic sections of higher resolution than other seismological data. We compared seismic record sections and travel time picks from continental areas in the offset interval from 300 to 2500 km. Only a few high-density seismic experiments at such long ranges have been carried out, and the profiles are thus unevenly distributed on the globe (Fig. 1 and Table 1). The travel times (Fig. 2A) fall into two distinct categories: (i) "cold areas," which are tectonically stable, aseismic regions, generally characterized by low heat flow, and (ii) "hot areas," which are tectonically unstable, seismically active regions with high heat flow.

There is only a slight difference in arrival time and linearity for the two regions at source-receiver offsets to ~500 km. At larger offsets, the difference in travel time through the continental mantle increases to a maximum of ~6 s for offsets larger than ~1500 km (*10*). All seismic sections show coherent, linear first arrivals out to ~8° offset, which indicates that the mantle is stratified to depths of ~100 km (zone I, Fig. 2C). The resolution or detection limit corresponds vertically to the seismic wavelength, which is of the order of 1 km, and horizontally to the Fresnell Zone diameter, which is of the order of 10 km. The P_n wave, refracted from underneath the Moho, is observable to offsets of 400 km, beyond which the general trends of travel time picks correspond to average velocities of 8.2 km/s in cold areas and 8.0 km/s in hot areas.

At offsets larger than ~800 km, the first breaks are delayed and the arrivals are scattered in the sense that seismic phases cannot be correlated, the amplitude variation is strong, and there is a strong coda of several seconds duration (zone II, Fig. 2C). This qualitative description applies to both cold and hot areas despite the different travel times. We interpret these arrivals as reflections from bodies in a low-velocity zone below depths of ~100 km. A high-density seismic section from the BABEL Project (*11*) shows that the horizontal extent of the individual reflecting bodies cannot be more than 10 to 20 km beneath the Baltic Shield (*9*).

The scattered arrivals extend to offsets of ~1800 km for hot areas, whereas the picks are linearly aligned beyond offsets of ~1300 km (1100 to 1500 km) for cold areas, which is indicative of the Lehmann discontinuity (zone III, Fig. 2C). Strong coherent, secondary arrivals at offsets beyond ~1700 km are indicative of the 400-km discontinuity, which is a global continental feature (zone IV, Fig. 2C).

Synthetic seismic sections (Figs. 3 and 4) illustrate these differences. They were calculated with the reflectivity method (*12*), which is based on one-dimensional, spherically or horizontally layered models of the Earth. Therefore, the synthetic sections provide qualitative images of the interference effects from the fine layering, even though they cannot describe true three-dimensional effects from scattering bodies.

Seismic record sections from the Baltic Shield for FENNOLORA shot point I (*13*) are examples from a cold area (Fig. 3, A and C). Linear seismic phases (P1 through P3) are interpreted as refractions from the stratified zone I above the 8° discontinuity. No phase correlation is possible between offsets of 800 and 1200 km, where the first arrivals follow the dashed curve in front of a strong coda of 4- to 6-s duration. The linear first arrivals at offsets beyond 1300 km indicate refractions from depths below ~180 km. The reflection from the 400-km discontinu-

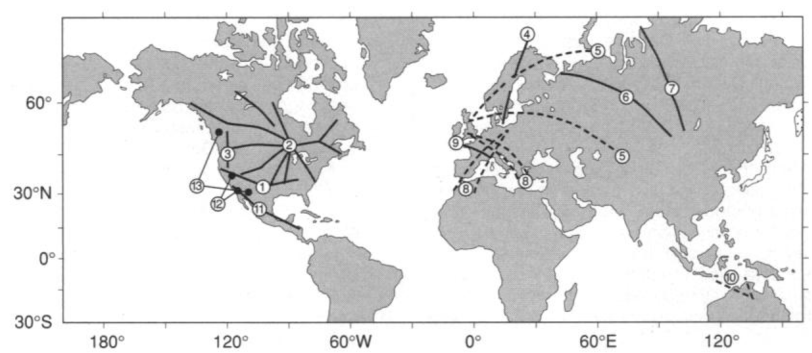

Fig. 1. Location of the analyzed high-resolution seismic profiles. Numbers refer to the list in Table 1.

H. Thybo, Geological Institute, University of Copenhagen, Øster Voldgade 10, DK-1350 Copenhagen K, Denmark.
E. Perchuć, Institute of Geophysics, Polish Academy of Sciences, ul.Księcia Janusza 64, PL-01452 Warsaw, Poland.

*To whom correspondence should be addressed.

ity is a secondary phase beyond 1650 km. The synthetic sections (Fig. 3, B and D) are qualitatively in agreement with the seismic sections except for minor differences in exact travel times and amplitude relations, for example, at the local advance in travel time from crustal structure at offsets between 1300 and 1500 km.

The extensional center of the Gulf of California is an example of a hot area from which the earthquake-based record section in Fig. 4A was selected (*14*). The first arrivals are scattered in arrival time and amplitude from the beginning of the section to an offset of 18°. The strong ringing of several seconds duration in this interval is modeled as a series of reflections from a layered structure. The synthetic section (Fig. 4C) and the seismic section appear to be similar, even though the scattering and its duration are not fully resolved, primarily because of the applied one-dimensional model. The arrival times are linear and the amplitudes vary smoothly for the strong phases from the 400-km and 650-km discontinuities, which shows that the offsets and onset times of the earthquakes are correctly estimated for the construction of the section, thus substantiating that the seismic phases are scattered between offsets of 9° and 18°.

Our analysis requires two fundamentally different velocity-depth distributions for hot and cold areas (Fig. 2C). The cold area model comprises four depth intervals in the uppermost mantle. Zone I extends from the crust-mantle boundary to a depth of ~100 km (90 to 120 km) and is characterized by subhorizontal layering in which the high-velocity layers have velocities between 8.0 and 8.7 km/s. Zone II is a low-velocity zone that extends to a depth of ~200 km (150 to 280 km), depending on the location. Arrival times and amplitudes of waves from this interval are scattered, which implies that

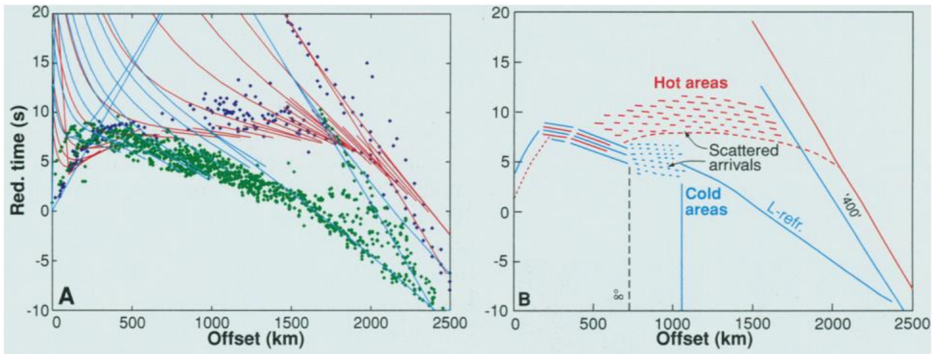

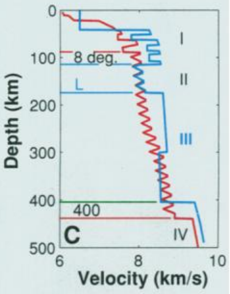

Fig. 2. (**A**) Selected travel time picks and calculated travel time branches for representative models of hot, tectonically active (purple points, red curves) and cold, tectonically quiet areas (green points, blue curves). Travel times are reduced by 8 km/s so that seismic phases with velocity of 8 km/s appear along horizontal lines. Travel time picks are from the projects described in Table 1, and calculated travel time curves are for the generalized models in (C). Only first breaks are included except for interpreted seismic phases from the 400-km discontinuity. There is an increasing time difference between picks from cold and hot areas from an offset of 500 km to a maximum difference of ~6 s at offsets beyond ~1500 km. (**B**) Generalized interpretation of the travel time picks in (A). The 8° discontinuity marks the transition from short duration, linear seismic phases to scattered seismic arrivals with a long duration coda. The refraction from below the Lehmann discontinuity (L-refr.) is a characteristic of cold areas and marks the transition from scattered character to linear arrivals. "400" indicates the 400-km discontinuity. (**C**) Generalized velocity models for cold and hot areas. Zones I to IV represent the four main depth intervals in the uppermost mantle, separated by the 8° discontinuity (8 deg.), the Lehmann discontinuity (L), and the 400-km discontinuity (400). Zone III and the Lehmann discontinuity are exclusively determined in cold areas.

Table 1. Sources of data (*3, 8, 10, 13, 14, 24*) analyzed for this study and origin of travel time picks plotted in Fig. 2A. NA, North America; WA, western North America; BS, Baltic Shield; EA, Eurasia; S, Siberia; EU, Europe; AI, Australia and Indonesia; NE, nuclear explosion; CE, chemical explosion; EQ, earthquakes; H, hot area; C, cold area. Numbers correspond to the seismic profiles in Fig. 1. Dashes indicate projects lacking acronyms.

Number	Region	Name of project	Source type	Model type
1	NA	GNOME	NE	HC†
2	NA	Early Rise	CE	CH‡
3	WA	–	CE	H
4	BS	FENNOLORA	CE*	C
5	EA	–	NE	C
6	EA	QUARZ	NE*	C
7	S	RIFT	NE*	C
8	EU	–	EQ	C
9	EU	Brest	CE*	C
10	AI	–	EQ*	H
11	WA	SCARLET	EQ*	H
12	WA	PAC-NW	EQ	H
13	WA	–	NE*	HC†

*Only selected travel time picks are shown in Fig. 2A. †Profiles from western (eastern and center) North America show hot (cold) character. ‡Profiles reaching into western North America show the characteristic delay of the hot model.

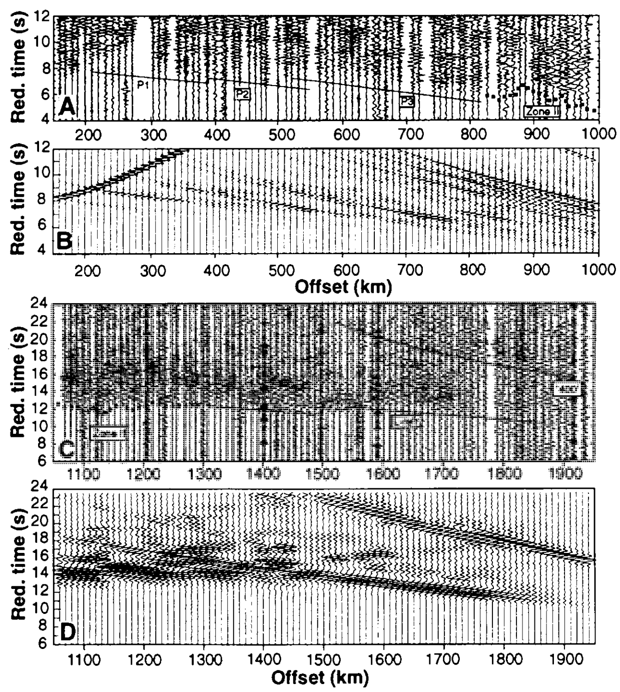

Fig. 3. (**A** and **C**) Seismic sections for FENNOLORA shot point I (*13*) from the "cold" Baltic Shield. The linear seismic phases P1 through P3 are from zone I. The scattering of first breaks from zone II beneath the 8° discontinuity is illustrated by solid squares. Refracted waves from below the Lehmann discontinuity are shown by "L-refr" and the reflection from the 400-km discontinuity by "400." The advance in travel time for the Lehmann refraction at offsets between 1300 and 1500 km is caused by local, near-surface structure. (**B** and **D**) Synthetic seismograms calculated by the reflectivity program (*12*) for the cold velocity model in Fig. 5A. The overall correlation between corresponding sections is very good, except for minor differences in exact arrival times caused by local structure. Notice the strong coda from zone II, the Lehmann refraction, and the reflection from the 400-km discontinuity. Reduction velocity is 8 km/s in (A) and (B) and 8.5 km/s in (C) and (D).

the mantle is inhomogeneous on a scale corresponding to the seismic wavelength and Fresnell Zone diameter. The Lehmann discontinuity to zone III is identified from a clear, linear, refracted seismic phase of smooth amplitude variation. The 400-km discontinuity is identified globally from a strong reflection and a linear refraction.

For hot areas, the velocities of the upper zone I are lower than for cold areas (Fig. 2C). Velocities below the 8° discontinuity at a depth of ~100 km are comparable to or slightly lower than those for cold areas. The scattered arrivals are observed out to long offsets, indicating that zone II at depth extends to near the 400-km discontinuity. No evidence has been observed for a Lehmann discontinuity into a high-velocity zone III for hot areas. The 400-km discontinuity is as pronounced in hot areas as in cold areas and shows only small depth variation.

Seismological data, with low frequency content and coarse spatial sampling, generally reveal low-velocity zones in the depth interval down to 400 km in hot areas but rarely in cold areas. Because of the limited resolution, such data cannot reveal a ~40 km–thick low-velocity zone at a depth of 100 km (*15*). Hence, the global velocity profiles PREM and IASP91 (*16*) do not include a low-velocity zone below ~100 km. Zones of low *P*- or *S*-wave velocity beneath a depth of ~100 km are identified from high-resolution surface wave or tomographic studies in Europe, Iberia, Tibet, western North America, and across the Urals in Russia (*17*). Hence, other seismic methods resolve the 8° discontinuity when data quality allows optimum resolution.

We conclude that a low-velocity zone at depths below ~100 km is a global feature of the continental mantle, because (i) it is identified from all available high-resolution data, except for one record section from the Canadian Shield and (ii) it does not contradict other data sets. It is likely that the 8° discontinuity is interrupted at subduction zones, active orogens, and rift zones. Most of the existing data were acquired in cold areas, and there is a need for further data acquisition, for example, from western North America, central Europe, and southeast Asia.

The stratified zone I with intermixed high- and low-velocity layers may consist of depleted and primitive, possibly metasomatically enriched, upper mantle rocks, mainly peridotites (*18*). The low velocities of zone II may indicate the presence of (i) volatile-free, high-temperature partial melt; (ii) volatile components that may exist as a separate fluid phase or dissolved in partial melt; or (iii) variations in mineralogy. The zone includes seismically reflecting bodies, and it cannot merely be explained by a difference in bulk composition to the surrounding intervals. The low velocities are probably caused by depth-constrained petrological changes, because the zone is everywhere at approximately the same depth for both hot and cold areas. The low velocities of the zone indicate that magma or fluids are present. Even small amounts of melts or fluids (<1 to 2%) can decrease the seismic velocity substantially (*19*). In view of expected geotherms, it is unlikely that dry peridotites or eclogites, in general, may generate partial melts from depths of ~100 km, whereas the presence of volatile components requires the existence of partial melts from this depth (Fig. 5B). A layer with partial melts has a low velocity and it may also generate scattered reflections. The interval may be interpreted as solid peridotites with patches of partial melt.

Patches enriched in a fluid or vapor phase could, in principle, also cause seismic scattering and low velocities. However, taking likely geotherms into consideration, the presence of volatile components in a peridotitic matrix would result in generation of partial melts (Fig. 5B). The seismically scattering bodies could also be caused by inclusions of contrasting rock types. Eclogite and piclogite have higher densities and comparable or higher velocities than peridotites (*20*). Therefore, this would imply a zone of higher velocity than interpreted, unless the interval was in a state of partial melt. Considering the low velocities, it is unlikely that differences in composition and mineralogy may be the primary explanation of the observations.

Continental geotherms for both hot and

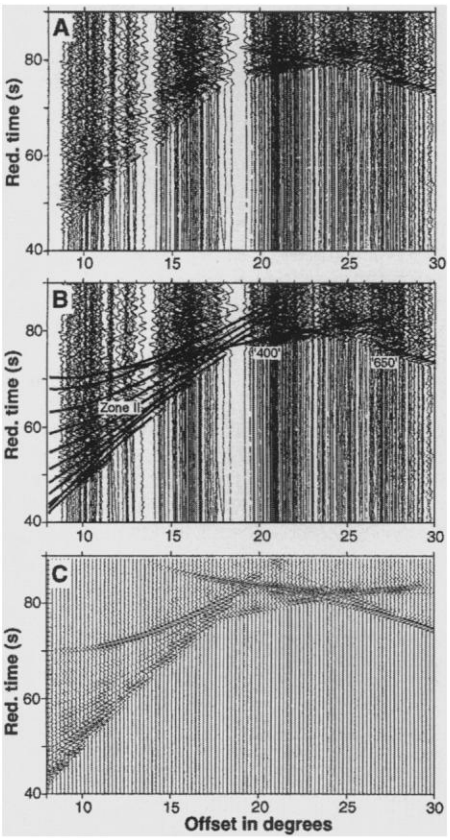

Fig. 4. (**A**) Seismic section from the "hot" Gulf of California (*14*). The section illustrates how the scattered reflections from zone II below the 8° discontinuity continues to far offsets (of 18°) where arrivals from the 400-km discontinuity dominates. The arrivals from the 400-km ("400") and the 650-km ("650") discontinuities are continuous, which shows that static shifts have been correctly applied. (**B**) Calculated travel times for the hot velocity model in Fig. 5A superimposed on the section. The scattered coda reflections from zone II are illustrated by a series of reflections. (**C**) Synthetic seismograms calculated with the reflectivity program (*14*) for the hot velocity model in Fig. 5A. There is a qualitative similarity between data and synthetic seismograms, even though the scattering from zone II may not be fully described with the applied one-dimensional, spherically layered model. There is no indication of arrivals from a Lehmann discontinuity in hot areas. Reduction velocity is 0.1° per second (~11.1 km/s).

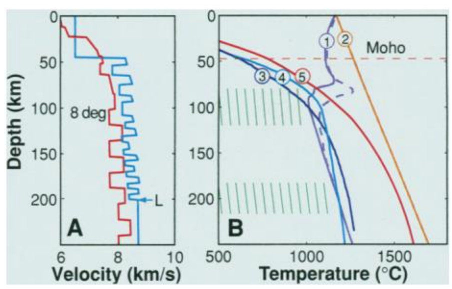

Fig. 5. Petrological model of the uppermost continental mantle of peridotitic composition based on expected geotherms. (**A**) Shown are the velocity models of the upper mantle that were applied for calculation of the synthetic seismograms in Figs. 3 and 4 for cold (blue) and hot (red) areas; 8 deg, 8° discontinuity; L, Lehmann discontinuity. (**B**) The temperature-depth diagram shows (1) two proposed solidus curves for peridotite with small amounts of C-H-O and (2) the solidus curve for dry peridotite (*21*). Generalized geotherms for cold and hot areas show: (3) an average geotherm for shield areas (*21*); (4) proposed geotherm for the northern Baltic Shield, which is a cold area (*9*); and (5) the average geotherm for hot areas (*23*). The geotherms cross solidus (1) at approximately the same depth of ~100 km because of the kink in the solidus, even though their general slopes are different. Partial melting is indicated below the 8° discontinuity, which explains why the scattered reflections from the low-velocity interval appear from approximately the same depth for cold and hot areas. Geotherm (4) crosses the solidus again at a depth around 200 km, illustrating that the Lehmann discontinuity is the lower termination of the partial melt zone. Geotherm (5) has no second crossing of the solidus, indicating that the zone of partial melt may extend to near the 400-km discontinuity.

cold areas cross the wet mantle solidus curve (*21*) around a depth of ~100 km (Fig. 5B). Because of the characteristic kink on the solidus curve, the zone of partial melting is reached at approximately the same depth in all regions, provided volatiles are present. The thickness of the zone depends on the thermal state of the area. The base of the zone may be near the 400-km discontinuity in hot areas, whereas it is shallower in cold areas. We interpret the base of the partially molten zone as the Lehmann discontinuity; its depth is thus an indicator of the thermal state of the mantle.

The presence of a partially molten layer beneath continents at a relatively constant depth of ~100 km will affect the rheology of the mantle. Such a soft layer is a likely detachment for relative motion between plates. The viscosity of the layer is probably low, which may explain the apparent differences in thickness of the lithosphere as determined from seismological and rheological studies (*22*). One seismic profile, the N-striking Early Rise profile, does not reveal the 8° discontinuity. This is likely because the mantle below the central Canadian shield is cold, as indicated by the thick elastic lithosphere.

REFERENCES AND NOTES

1. A. Mohorovicic, *Jahrb. Meteorol. Obs. Zagreb* **9**, 1 (1909); H. Jeffreys, *Mon. Not. R. Astron. Soc. Geophys. Suppl.* **3**, 401 (1936); M. Niazi and D. L. Anderson, *J. Geophys. Res.* **70**, 4633 (1965).
2. I. Lehmann, *Ann. Geophys.* **15**, 93 (1959); ______, *Bull. Seismol. Soc. Am.* **54**, 123 (1964).
3. R. P. Masse, *Bull. Seismol. Soc. Am.* **63**, 911 (1973); S. K. Dey-Sarkar and R. A. Wiggins, *J. Geophys. Res.* **81**, 3619 (1976); K. Priestley, J. Cipar, A. Egorkin, N. Pavlenkova, *Geophys. J. Int.* **118**, 369 (1994); J. Mechie *et al.*, *Phys. Earth Planet. Inter.* **79**, 269 (1993).
4. P. M. Shearer, *Nature* **344**, 121 (1990).
5. S.-I. Karato, *Geophys. Res. Lett.* **19**, 2255 (1992); J. B. Gaherty and T. H. Jordan, *Science* **268**, 1468 (1995).
6. I. B. Lambert and P. J. Wyllie, *Nature* **219**, 1240 (1968); *Science* **169**, 764 (1970); A. L. Hales, *Geophys. J. Int.* **105**, 355 (1991).
7. J. Ansorge and St. Mueller, *Z. Geophys.* **39**, 385 (1973); K. Fuchs and L. P. Vinnik, *Geodyn. Ser. Am. Geophys. Union* **8**, 81 (1982).
8. A. Hirn *et al.*, *Z. Geophys.* **39**, 363 (1973).
9. E. Perchuć and H. Thybo, *Tectonophysics* **253**, 227 (1996).
10. C. Romney *et al.*, *Bull. Seismol. Soc. Am.* **52**, 1057 (1962).
11. BABEL Working Group, *Geophys. Res. Lett.* **18**, 645 (1991).
12. K. Fuchs and G. Müller, *Geophys. J. R. Astron. Soc.* **23**, 417 (1971).
13. F. Hauser, C. Prodehl, M. Schimmel, *Geophys. Inst. Open File Report 90-2* (University of Karlsruhe, Germany, 1990).
14. M. Walck, *Geophys. J. R. Astron. Soc.* **76**, 697 (1984).
15. H. J. van Heijst, R. Sneider, R. Nowack, *Geophys. J. Int.* **118**, 333 (1994).
16. A. M. Dziewonski and D. L. Anderson, *Phys. Earth Planet. Inter.* **25**, 297 (1981); B. L. N. Kennett and B. Engdahl, *Geophys. J. Int.* **105**, 429 (1991).
17. A. Zielhuis and G. Nolet, *Science* **265**, 79 (1994); J. Badal, V. Corchete, G. Payo, L. Pujades, J. A. Canas, *Geophys. J. Int.* **124**, 591 (1996); B. A. Romanovicz, *J. Geophys. Res.* **87**, 6865 (1982); R. Zeng, Z. Ding, Q. Wu, *Pure Appl. Geophys.* **145**, 423 (1995); L. J. Burdick, *J. Geophys. Res.* **86**, 5926 (1981); G. Poupinet *et al.*, *Tectonophysics*, in press.
18. K. Fuchs, *Tectonophysics* **56**, 1 (1983).
19. G. M. Mavko, *J. Geophys. Res.* **85**, 5173 (1980); H. Sato, I. S. Sacks, T. Murase, *ibid.* **94B**, 5689 (1989).
20. D. L. Anderson, in *Continental Mantle*, M. A. Menzies, Ed. (Oxford Science Publications, Oxford, 1990), pp. 1–30.
21. P. J. Wyllie, *J. Geophys. Res.* **85**, 6902 (1980); ______, *J. Geodyn.* **20**, 429 (1995).
22. T. M. Bechtel *et al.*, *Nature* **343**, 636 (1990); R. Hartley, A. B. Watts, J. D. Fairhead, *Earth Planet. Sci. Lett.* **137**, 1 (1996); K. Lambeck, P. Johnston, M. Nakada, *Geophys. J. Int.* **103**, 451 (1990).
23. J. Leliwa-Kopystynski and R. Teisseyre, Eds., *Constitution of the Earth's Interior* (PWN-Elsevier, Amsterdam, 1984), p. 171.
24. H. M. Iyer, L. C. Parkiser, D. J. Stuart, D. H. Warren, *J. Geophys. Res.* **74**, 4409 (1969); D. P. Hill, *Geol. Soc. Am. Bull.* **83**, 1639 (1972); J. W. Given and D. V. Helmberger, *J. Geophys. Res.* **85**, 7183 (1980); D. Mayer-Rosa and St. Mueller, *Z. Geophys.* **39**, 395 (1973); J. R. Bowman and B. L. N. Kennett, *Geophys. J. Int.* **101**, 411 (1990); S. Malone, personal communication; J. E. Vidale, X.-Y. Ding, S. P. Grand, *Geophys. Res. Lett.* **22**, 2557 (1995).

25. We thank A. Berthelsen (Copenhagen), F. Surlyk (Copenhagen), and P. J. Wyllie (Pasadena, CA) for comments to an earlier version of the manuscript. Supported by the Danish Natural Science Research Council and the Polish State Committee of Scientific Research.

11 October 1996; accepted 17 January 1997

Paleomagnetic Evidence of a Low-Temperature Origin of Carbonate in the Martian Meteorite ALH84001

Joseph L. Kirschvink, Altair T. Maine, Hojatollah Vali

Indirect evidence for life on Mars has been reported from the study of meteorite ALH84001. The formation temperature of the carbonates is controversial; some estimates suggest 20° to 80°C, whereas others exceed 650°C. Paleomagnetism can be used to distinguish between these possibilities because heating can remagnetize ferrimagnetic minerals. Study of two adjacent pyroxene grains from the crushed zone of ALH84001 shows that each possesses a stable natural remanent magnetization (NRM), implying that Mars had a substantial magnetic field when the grains cooled. However, NRM directions from these particles differ, implying that the meteorite has not been heated significantly since the formation of the internal crushed zone about 4 billion years ago. The carbonate globules postdate this brecciation, and thus formed at low temperatures.

McKay *et al.* (*1*) proposed that carbonate globules in the Antarctic meteorite ALH84001 may contain relict evidence of early life on Mars. This meteorite is an orthopyroxene cumulate (pyroxenite) that crystallized 4.5 billion years ago (Ga) (*2, 3*) and experienced shock metamorphism and formation of the internal crushed zone about 4.0 Ga (*4, 5*). It contains carbonate globules that apparently formed after this event (*6, 7*) but before the impact that presumably launched the sample from the surface of Mars approximately 15 million years ago (*8*). The interpretation (*1*) that these carbonates contain traces of ancient life requires that they formed at low temperatures, but their temperature of formation has been uncertain. An aqueous environment between 20° and 80° C is suggested by stable-isotope studies (*9*) and the co-occurrence of magnetite, iron monosulfides, and carbonate (*1*), whereas petrographic and electron microprobe results (*10, 11*) have been interpreted in support of carbonate formation temperatures of 650° to 700°C. Bradley *et al.* (*12*), for example, identified needle-like magnetite whiskers with occasional twins in the carbonate phase, and interpret them as high-temperature vapor phase deposits. However, needle-like magnetite crystals of similar size and shape are also produced biologically on Earth (*13*), as are twinned crystals (*14*).

Because magnetic minerals lock in the magnetic field direction when they cool below their critical blocking temperatures, paleomagnetism can be used to determine the thermal history of the ALH84001 meteorite (*15*). Rock-magnetic studies of other martian meteorites are consistent with the presence of a magnetic field on Mars of 1 to 10 μT in strength, at least as recently as 1.3 Ga (*16, 17*), and evidence from the Earth (*18*) and the moon (*19*) is consistent with the presence of a strong internal dynamo in the terrestrial planets early in their history. The Neél (~Curie) temperature of pure magnetite is 580°C, and the Neél temperatures of the pyrrhotite mineral family are

J. L. Kirschvink and A. T. Maine, Division of Geological and Planetary Sciences, California Institute of Technology, 170-25, Pasadena, CA 91125, USA.
H. Vali, Department of Earth and Planetary Sciences, McGill University, Montreal, Quebec H3A 2A7, Canada.